Inorganic Chemistry

pubs.acs.org/IC

Article

Hydrogenation Properties of $Mg_{83.3}Cu_{7.2}Y_{9.5}$ with Long Period Stacking Ordered Structure and Formation of Polymorphic γ-MgH_2

Véronique Charbonnier,* Kohta Asano, Hyunjeong Kim, and Kouji Sakaki

Cite This: https://dx.doi.org/10.1021/acs.inorgchem.0c02080

Read Online

ACCESS | Metrics & More | Article Recommendations | Supporting Information

ABSTRACT: Nanosizing is known to affect the hydrogenation properties of magnesium. For this reason, the long period stacking ordered (LPSO) structures, made of the stacking of nanolayers of magnesium and nanolayers of Mg-A-B (with A = rare earth and B = transition metal), were herein considered. A $Mg_{83.3}Cu_{7.2}Y_{9.5}$ LPSO compound with 18*R* structure was successfully synthesized. Its hydrogenation properties were investigated at temperatures between 150 and 400 °C. The X-ray diffraction (XRD) analysis indicates that the LPSO structure decomposes into magnesium hydride, yttrium hydride, and an intermetallic compound (Mg_2Cu or $MgCu_2$). The pressure composition (PC) isotherm for $Mg_{83.3}Cu_{7.2}Y_{9.5}$ at 400 °C combined with XRD analysis allows one to understand the three-step hydrogenation pathway, detailed in this paper. At this hydrogenation temperature, the fully hydrogenated compound contains magnesium hydride exclusively crystallized in the most stable tetragonal structure (100% of α-MgH_2 was formed). When the pristine LPSO was hydrogenated at lower temperature, the amount of α-MgH_2 decreased, while its polymorphic structure, γ-MgH_2, appeared. Finally, hydrogenation of $Mg_{83.3}Cu_{7.2}Y_{9.5}$ at 150 °C led to the formation of γ-MgH_2 with a high phase fraction (82% of γ-MgH_2/MgH_2). These results suggest that the crystallographic structure of the magnesium hydride can be controlled by the hydrogenation temperature of LPSO compounds.

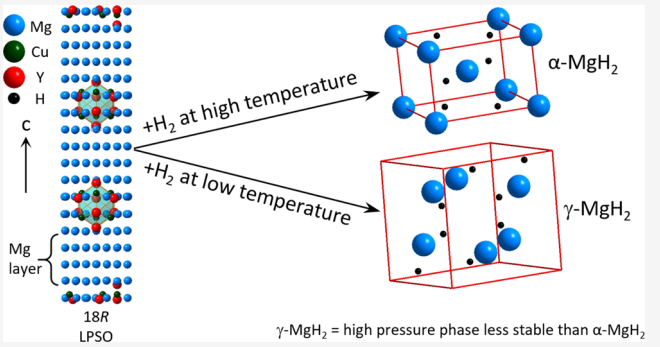

1. INTRODUCTION

Hydrogen is a promising energy carrier. One of the bottlenecks in hydrogen technologies is hydrogen storage. Magnesium is a light, inexpensive, and abundant metal extensively investigated for this purpose. Upon hydrogenation, it forms tetragonal α-MgH_2 with a high hydrogen content of 7.6 wt %.[1,2] However, this hydride is thermodynamically very stable: its decomposition temperature at 1 bar is 278 °C. This temperature is too high for mobile application.[3] In addition to its high stability, magnesium hydride also suffers from low kinetics for hydrogen absorption and desorption, so that even higher temperatures are required to absorb and desorb hydrogen (350−400 °C).[4]

In order to destabilize the hydride phase and improve its reaction kinetics, several processes are under investigation worldwide, including nanostructuration,[1,5] addition of catalysts,[1,6−9] and alloying.[10] It is worth noticing that, upon hydrogenation, the formation of polymorphic MgH_2 may occur. MgH_2 has several polymorphic forms: orthorhombic γ-MgH_2 with an α-PbO_2-type structure ($Pbcn$)[11−13] and cubic β-MgH_2 with a PdF_2-type structure ($Pa\bar{3}$).[12] They are known for being metastable and, thus, their formation should lead to lower desorption temperature and faster kinetics. First principle calculations for the polymorphic structures of MgH_2 revealed that the desorption enthalpy change ΔH is higher for β-MgH_2 (−44.4 kJ/mol H_2[14]) and for γ-MgH_2 (−52.8 kJ/mol H_2[14] or −44.66 kJ/mol H_2[15]) than for α-MgH_2 (−53.2 kJ/mol H_2[14]). Note that these values must be taken with care because $\Delta H(\alpha\text{-}MgH_2)$ = −53.2 kJ/mol H_2 is overestimated when compared to the experimental value of −74.5 kJ/mol H_2.[16]

Those two polymorphic structures (β- and γ-MgH_2) are interesting from the point of view of destabilization of magnesium hydride, since they are thermodynamically unstable compared to α-MgH_2. On the other hand, this also explains that they are difficult to synthesize. Indeed, the calculated pressure−temperature phase diagram of MgH_2 shows that ultrahigh pressure (on the order of the GPa) is needed to form β- or γ-MgH_2.[17] This was confirmed experimentally by the application of 2.5 GPa of pressurized inert gas (Ar or He) on α-MgH_2.[12,13] Other techniques, such as high pressure torsion (HPT)[14] and ball-milling,[1,15,18,19] also

Received: July 14, 2020

highlighted the transformation (or partial transformation) of α-MgH_2 into γ-MgH_2. Both techniques imply external mechanical deformation, leading to the formation of defects, strain, and reduction of crystallite size. The formation of γ-MgH_2 was also achieved by hydrogenation of Mg-thin films.[20−22] It was attributed to a smaller dimension of film and strain generated by the clamping effect of the thin film to the substrate.[20] Finally, to synthesize γ-MgH_2, three key points emerge from these methods (mechanical deformation and hydrogenation of thin films): large strain, structural defects, and nanosizing.

Long period stacking ordered (LPSO) compounds (Figure 1) were originally studied for their outstanding mechanical properties,[23] but the high content of magnesium in these LPSO structures makes them possible candidates for hydrogen storage. They are Mg-based compounds containing a small amount of rare earth (A) and transition metal (B). Up to now, three different stacking sequences of LPSO were identified: 10*H*, 18*R*, and 14*H*.[24] Crystal structures were proposed on the basis of transmission electron microscopy (TEM) results.[25−29] Table 1 summarizes the ideal compositions and proposed space groups of the LPSO structures. As evidenced by their crystallographic structures (Figure 1), the LPSO compounds are made by stacking hcp-Mg layers (gray layers) and Mg-A-B layers (red layers) along the *c*-axis. These structures resemble multilayered thin films but with extremely thin layers (on the order of nanometers). Therefore, there is a possibility that the hcp-Mg layer forms MgH_2 with different crystal structures from most stable tetragonal α-MgH_2, leading to a lower desorption temperature of hydrogen.

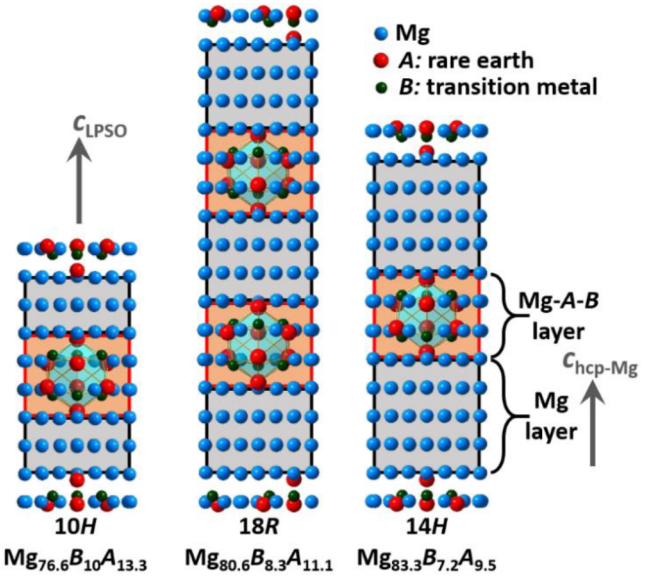

Figure 1. Crystal structures of LPSO compounds draw on the basis of TEM results: 10*H* with space group *Cmce*,[26] 18*R* with space group $P3_212$,[28] and 14*H* with space group $P6_3/mcm$.[28] The polyhedron in the Mg-A-B layer is a B_6A_8 cluster. The composition is indicated below each crystal structure.

In this study, the Mg−Cu−Y system was chosen because Cu,[30] Y, and YH_x[31−33] are known for their catalytic effect on hydrogenation of Mg. Herein, we investigate the hydrogenation properties of the $Mg_{83.3}Cu_{7.2}Y_{9.5}$ LPSO compound. This study shows a simple and new synthesis route for a large amount of orthorhombic γ-MgH_2.

2. EXPERIMENTAL SECTION

Chunks of Mg (99.9%) from Kojundo Chemical Laboratory Co., Ltd., Cu (99.99%) from Furuuchi Chemical Co., and Y (99.9%) from Nippon Yttrium Co., Ltd. were used to synthesize $Mg_{83.3}Cu_{7.2}Y_{9.5}$. Due to its high vapor pressure, an excess of 7 wt % of magnesium was added. The elements were melted together in an induction furnace under a helium atmosphere. The obtained ingot was wrapped in aluminum foil and subsequently annealed for 50 h at 400 °C under an argon atmosphere.

X-ray diffraction (XRD) analysis was performed with a Rigaku 2500 V diffractometer with Cu Kα radiation in a 2θ range from 3° to 80° with a step size of 0.02°. The FULLPROF program[34] based on the Rietveld method[35] was used to determine crystallographic properties and phase amounts.

The compound was observed with a S-3400N scanning electron microscope (SEM) from Hitachi. Back scattered electron (BSE) mode and an energy dispersive X-ray (EDX) detector were used. A piece of ingot was embedded in a resin and mechanically polished using diamond paste. After polishing, conductive paste was used in order to ensure the electronic conductivity.

Pressure composition (PC) isotherms were measured using Sieverts' method. The ingot was filed into powder in air. Approximately 1 g of powder was introduced in a stainless steel vessel and heated at 400 °C for 5 h in an argon atmosphere. It was evacuated, and the measurement was started. At the end of the measurement, the temperature was kept and the sample holder was evacuated under dynamic vacuum for several hours.

3. RESULTS

3.1. Phase Determination and Structural Properties.

Figure 2 shows the XRD pattern of $Mg_{83.3}Cu_{7.2}Y_{9.5}$. This composition is close to stoichiometric 14*H* phase determined by TEM analysis.[25,26,28] The low angle diffraction peak at 5.6° corresponds to the interplanar distance d_{hkl} of 1.58 nm. This indicates that a long period crystallographic structure is formed. This interplanar distance is consistent with the 18*R* structure of LPSO[36] and much shorter than that for the 14*H* structure (1.81 nm) as shown in Table 1. To confirm the

Table 1. Tabulated Compositions and Proposed Space Groups for LPSO Compounds with 10*H*, 18*R*, and 14*H* Structures[a]

	Mg (at %)	B (at %)	A (at %)	B/A	*hkl*	d_{hkl} (nm)	2θ (deg)	proposed space groups	ref.
10*H*	76.7	10	13.3	0.75	002	1.31	6.8	*Cmce*	26
					002	1.30	6.8	$P6_3/mcm$	27
18*R*	80.6	8.3	11.1	0.75	001	1.56	5.6	*C*2/*m*	29
					002	1.56	5.6	*C*2/*c*	26
					003	1.56	5.6	$P3_212$	28
14*H*	83.3	7.2	9.5	0.75	002	1.81	4.9	$P6_3/mcm$	28, 29
					002	1.82	4.9	$P6_322$	26

[a]B is a transition metal, and A is a rare earth. The 2θ column indicates the position of the first diffraction peak for XRD measurements with Cu Kα radiation.

https://dx.doi.org/10.1021/acs.inorgchem.0c02080
Inorg. Chem. XXXX, XXX, XXX−XXX

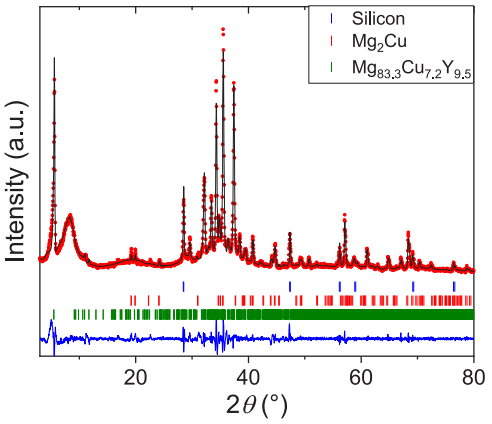

Figure 2. XRD pattern for $Mg_{83.3}Cu_{7.2}Y_{9.5}$ after annealing treatment at 400 °C for 50 h. The *C2/m* space group determined by Saal and Wolverton[29] was used for the Le Bail refinement of $Mg_{83.3}Cu_{7.2}Y_{9.5}$ with the 18*R* structure.

nature of the main phase, Le Bail refinement was performed.[37] A small amount of silicon was added to the sample as a reference in order to determine the displacement of the sample. Then, it was fixed, and the Le Bail refinement of the main phase was started. The three different space groups proposed for the 18*R* structure and presented in Table 1 (*C2/m*, *C2/c*, and $P3_212$) were tried. The *C2/m* space group gave the best goodness of fit, and the derived cell parameters are a = 11.157(1) Å, b = 19.478(2) Å, c = 16.620(3) Å, and β = 77.28(1)°. Most of the diffraction peaks were indexed by this 18*R* structure, while some of the tiny peaks, indicated in Figure 2, correspond to the Mg_2Cu phase.

SEM−BSE micrographs are shown in Figure 3. The global composition derived from SEM−EDX analysis at low

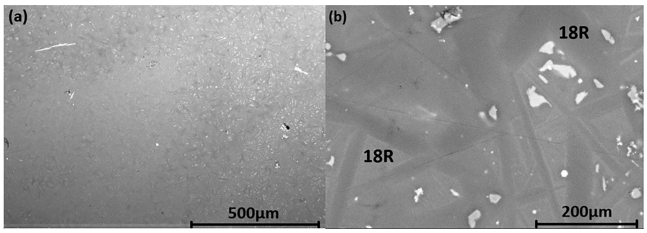

Figure 3. SEM images of $Mg_{83.3}Cu_{7.2}Y_{9.5}$ annealed at 400 °C for 50 h at low magnification (a) and high magnification (b).

magnification (Figure 3a) is $Mg_{83.8\pm0.2}Cu_{7.4\pm0.3}Y_{8.8\pm0.1}$, which is close to the target composition. High magnified SEM−BSE micrographs and EDX analysis show different phases. The main area is light gray and corresponds to $Mg_{83.31\pm0.07}Cu_{7.39\pm0.05}Y_{9.30\pm0.03}$. The dark gray area having a composition of $Mg_{85.9\pm0.7}Cu_{6.3\pm0.2}Y_{7.8\pm0.5}$ has a Mg content slightly higher than the light gray area. As an impurity phase, a white area, with $Mg_{70.7\pm0.03}Cu_{14.4\pm0.3}Y_{14.9\pm0.4}$ composition, was also observed. Light gray and dark gray areas have a composition close to the stoichiometric 14*H* compound. However, the XRD analysis does not show the 14*H* structure, whereas the 18*R* structure is clearly present. Our results suggest that our 18*R* phase contains more Mg than the stoichiometric 18*R* phase (Table 1). This tendency is consistent with refs 38 and 39. We will discuss this compositional difference from the stoichiometric 18*R* phase later.

3.2. Hydrogenation Properties and Phase Decomposition upon Hydrogenation. Figure 4a shows the PC isotherm of $Mg_{83.3}Cu_{7.2}Y_{9.5}$ measured at 400 °C. 1.86 H/M (atomic ratio of hydrogen and metal atoms) was absorbed and 1.62 H/M was desorbed, which corresponds to 4.7 wt % of reversible capacity. When one takes a closer look at the details, a three step-reaction for hydrogenation is observed: hydrogen absorption in low hydrogen pressure (below 0.05 MPa) and two plateaus at 1.2 and 4 MPa. In order to understand the three step-reaction, XRD patterns were measured at different states of charging (Figure 4a, points 1 to 4). The detailed structure information obtained by Rietveld refinement is shown in Table 2. Note that a small amount of Y_2O_3 is always observed, indicating contamination from the air.

The sample hydrogenated at 400 °C under 0.5 MPa of hydrogen pressure (point 1) shows that the LPSO structure already decomposed and formed YH_2, Mg, and Mg_2Cu (Figure 4b). At this point, MgH_2 was not observed. The lattice constants of Mg and YH_2 are almost the same as the literature values. After further hydrogenation (point 2), the XRD analysis shows that the main phases are α-MgH_2, YH_3, and Mg_2Cu (Figure 4c). Therefore, the plateau at 1.2 MPa corresponds both to the further hydrogenation of YH_2 into YH_3 and to the hydrogenation of Mg in MgH_2. Then, pristine $Mg_{83.3}Cu_{7.2}Y_{9.5}$ was fully hydrogenated at 400 °C under 4 MPa of hydrogen pressure (point 3). The XRD pattern highlights the presence of α-MgH_2, YH_3, and $MgCu_2$ and traces of YH_2 (2.5 wt %) (Figure 4d). The plateau at 4 MPa can thus be attributed to the decomposition of Mg_2Cu into MgH_2 and $MgCu_2$. The structure of MgH_2, which was formed here, is tetragonal ($P4_2/mnm$), and its cell parameters are very close to the literature values, although hydrogenation of Mg-X systems (X = Sc,[40] Ti[41]) can lead to the formation of $(Mg,X)H_2$ with an $Fm\bar{3}m$ space group (FCC structure). Similarly, the structure of YH_3 was hexagonal even though Mg-doped Y can form FCC YH_3.[42] These structural features and the lattice constants indicate that Mg and Y were not mixed with each other. Finally, the XRD pattern recorded after PC isotherm measurement at 400 °C (point 4) shows that dehydrogenation products were YH_2, Mg, and Mg_2Cu (Figure 4e). In the whole process, the change in phase fraction estimated by Rietveld refinements was reasonable: the capacities derived from Rietveld refinement (Table 2) are very close to the ones observed by PC isotherm measurement (Figure 4a).

After the first hydrogenation at 400 °C, the temperature was kept and the sample holder was evacuated under dynamic vacuum for several hours. Then, a second hydrogenation was performed at 150 °C under 5 MPa. The maximal hydrogen content after the second hydrogenation at 150 °C is 1.42 H/M. It decreased by 0.44 H/M compared to the first hydrogenation at 400 °C. No hydrogen desorption was observed at this temperature. As shown in Figure 5, main phases are α-MgH_2, YH_3, and Mg_2Cu. Traces of unreacted YH_2 and Mg are also present. At this condition, the reaction products were almost the same as those at 400 °C although Mg_2Cu was not hydrogenated into α-MgH_2 and $MgCu_2$.

In order to understand the temperature effect on hydrogenation of $Mg_{83.3}Cu_{7.2}Y_{9.5}$, a PC isotherm of pristine $Mg_{83.3}Cu_{7.2}Y_{9.5}$ was measured at 150 °C (Figure 6a). During the first cycle, one single plateau is lying at 0.14 MPa. Hydrogen was absorbed up to 1.43 H/M, but hydrogen desorption was not observed. The sample cell was subsequently evacuated under dynamic vacuum at 150 °C

https://dx.doi.org/10.1021/acs.inorgchem.0c02080
Inorg. Chem. XXXX, XXX, XXX−XXX

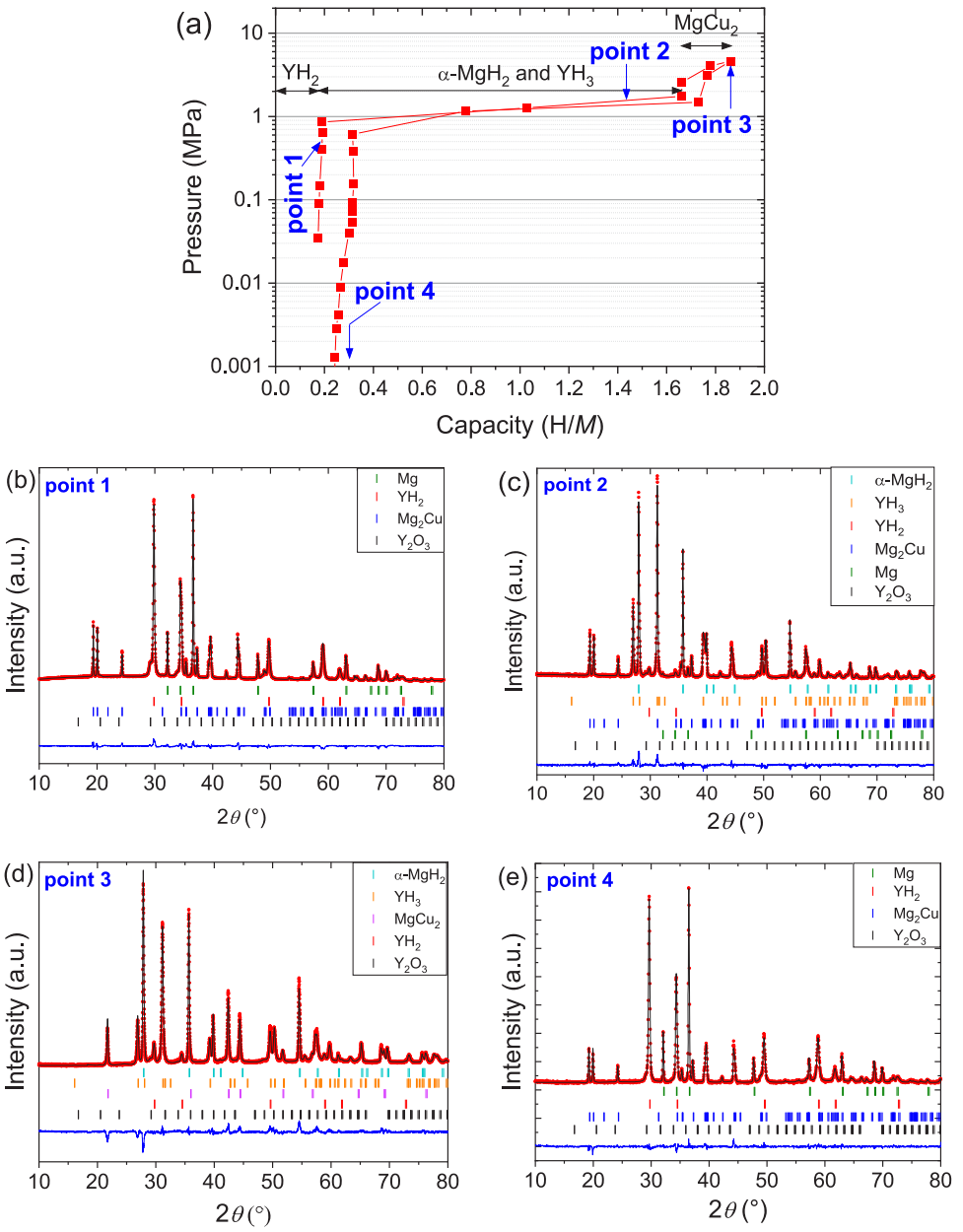

Figure 4. (a) PC isotherm for $Mg_{83.3}Cu_{7.2}Y_{9.5}$ measured at 400 °C. Points 1, 2, 3, and 4 indicate, respectively, the conditions for the measurements of Rietveld refined XRD patterns of $Mg_{83.3}Cu_{7.2}Y_{9.5}$: (b) hydrogenated at 400 °C under 0.5 MPa, (c) hydrogenated at 400 °C under 1.5 MPa, (d) hydrogenated at 400 °C under 4 MPa, and (e) after PC isotherm measurement at 400 °C.

for several hours. Second and third cycles were measured, but no absorption occurred. This suggests that evacuation under dynamic vacuum does not allow hydrogen desorption. Indeed, high temperatures are required to desorb hydrogen from MgH_2 and YH_2. At 150 °C, the desorption pressure for MgH_2 is about 0.0007 MPa and desorption kinetics is slow. As for YH_2, it was shown that its desorption starts at 650 °C under dynamic vacuum.[43] Figure 6b shows the XRD pattern recorded after the first PC isotherm measurement and subsequent evacuation. This pattern is completely different from those in Figures 4d and 5.

The two diffraction peaks around 20° indicate that Mg_2Cu remained after hydrogenation. The diffraction peak at 5.6°, characteristic of 18*R* LPSO, is still present, but its intensity drastically decreased. In order to analyze the diffraction pattern in detail, the powder was crushed in ethanol and only the supernatant powder was used for Rietveld refinement. This fine supernatant powder did not contain 18*R* LPSO (because LPSO is a very coarse powder, it sank), and MgO and Y_2O_3 were introduced during this operation; however, the main feature of the diffraction pattern mostly remained.

First, the Rietveld refinement was attempted by using a similar strategy as in Figure 5. The quality of the refinement was poor (Figures 6c and S1a): the position of the main peak at 31° is close to that for YH_3; however, the intensity at 31° is underestimated, and those at 26.8 and 27.9° are overestimated. Then, the orthorhombic γ-MgH_2 was considered for Rietveld refinement (Figures 6d and S1b). Note that, now, the calculated intensities of the main diffraction peak at 31° and other peaks (especially at 26.8° and 27.9°) match the observed intensities. In addition, the peak at 25.3°, which was not indexed using the first refinement models, is indexed by γ-

https://dx.doi.org/10.1021/acs.inorgchem.0c02080
Inorg. Chem. XXXX, XXX, XXX−XXX

Table 2. Results of Rietveld Refinement of $Mg_{83.3}Cu_{7.2}Y_{9.5}$ after Hydrogenation at 400 °C under 0.5 MPa (Figure 4b), 400 °C under 1.5 MPa (Figure 4c), 400 °C under 4 MPa (Figure 4d), PC Isotherm Measurement at 400 °C (Figure 4e), and Rehydrogenation at 150 °C (Figure 5)[a]

	Mg $P6_3/mmc$	α-MgH_2 $P4_2/mnm$	YH_2 $Fm\bar{3}m$	YH_3 $P\bar{3}c1$	Mg_2Cu $Fddd$	$MgCu_2$ $Fd\bar{3}m$	Y_2O_3 $Ia\bar{3}$
After Hydrogenation at 400 °C under 0.5 MPa							
wt %	51.1(2)		20.7(1)		24.3(1)		3.9(2)
a (Å)	3.20959(4)		5.1848(2)		5.2786(3)		10.581(3)
b (Å)	a		a		9.0616(5)		a
c (Å)	5.2117(2)		a		18.338(1)		a
L (nm)	[b]		90(10)		100(6)		[c]
ε (%)	[b]		0.42		0.077		[c]
C (H/M)				0.15			
χ^2 (%)				7.91			
After Hydrogenation at 400 °C under 1.5 MPa							
wt %	2.5(1)	50.4(3)	1.1(1)	21.6(1)	23.5(2)		0.9(1)
a (Å)	3.208(1)	4.5154(4)	5.194(1)	6.3534(6)	5.2816(4)		10.57(1)
b (Å)	a	a	a	a	9.068(1)		a
c (Å)	5.217(3)	3.0206(1)	a	6.6099(7)	18.351(2)		a
L (nm)	[c]	230(70)	[c]	75(5)	71(6)		[c]
ε (%)	[c]	0.10	[c]	0.22	0.060		[c]
C (H/M)				1.57			
χ^2 (%)				2.03			
After Hydrogenation at 400 °C under 4 MPa							
wt %		60.2(3)	2.4(1)	19.1(1)		16.3(1)	2.0(1)
a (Å)		4.5190(2)	5.197(1)	6.3598(4)		7.0597(3)	10.60(1)
b (Å)		a	a	a		a	
c (Å)		3.0235(2)	a	6.6123(5)		a	
L (nm)		67(3)		29(1)		40(2)	[c]
ε (%)		0.080		0.16		0.19	[c]
C (H/M)				1.91			
χ^2 (%)				5.01			
After PCT at 400 °C							
wt %	53.3(4)		23.3(2)		22.4(3)		1.0(1)
a (Å)	3.2112(2)		5.1992(4)		5.2785(7)		10.59(1)
b (Å)	a		a		9.075(1)		a
c (Å)	5.2155(4)		a		18.349(2)		a
L (nm)	83(7)		50(3)		61(6)		[c]
ε (%)	0.095		0.39		0.078		[c]
C (H/M)				0.17			
χ^2 (%)				1.65			
After PCT at 400 °C and Hydrogenation at 150 °C							
wt %	3.3(2)	55.2(6)	13.7(2)	8.6(2)	18.5(3)		0.7(1)
a (Å)	3.209(2)	4.5187(6)	5.1992(7)	6.361(2)	5.282(1)		10.603(8)
b (Å)	a	a	a	a	9.078(2)		a
c (Å)	5.228(6)	3.0228(4)	a	6.604(3)	18.360(5)		a
L (nm)	[c]	43(3)	19(2)	19(2)	[c]		[c]
ε (%)	[c]	0.13	0.38	0.098	[c]		[c]
C (H/M)				1.60			
χ^2 (%)				4.06			

[a] L is the crystallite size (diameter); C indicates the hydrogen capacity (derived from weight percent of each phase); ε is the strain; χ^2 is the goodness of fit. [b] The diffraction peaks are almost as sharp as the silicon reference used to determine instrumental parameters. The contributions of the crystallite size and strain to the full width at half maximum is thus very low, and their value has no physical meaning. [c] The crystallite size and strain are not given because the phase fraction is too small and/or the diffraction peaks overlap with other phases, making it difficult to obtain values with a physical meaning.

MgH_2. Rietveld refinement (Figure 6d and Table 3) shows that a high fraction of γ-MgH_2 was formed (≈55 wt %). This value corresponds to 82% of γ-MgH_2/MgH_2. One can notice the large value of the a cell parameter and cell volume of γ-MgH_2 compared to the reported value of pure γ-MgH_2 ($\Delta a/a$ = +2.6%, $\Delta V/V$ = +2.39%). This is likely to be triggered by internal strain, resulting from the low temperature hydrogenation process, and will be further discussed later. In addition, it suggests that the magnesium is fully hydrogenated, so that the hydrogen content of the obtained γ-MgH_2 is close to 2.0 H/M. These results clearly indicate that polymorphic γ-MgH_2 was formed upon hydrogenation of $Mg_{83.3}Cu_{7.2}Y_{9.5}$ at 150 °C and under a low-pressure condition (0.14 MPa). Note that the lattice parameters of α-MgH_2 and YH_3 are almost the

https://dx.doi.org/10.1021/acs.inorgchem.0c02080
Inorg. Chem. XXXX, XXX, XXX−XXX

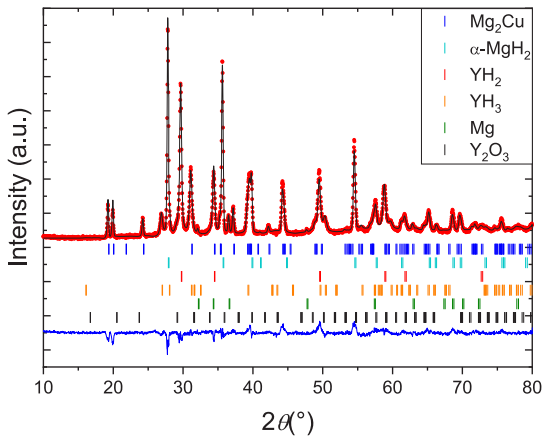

Figure 5. Rietveld refined XRD pattern of $Mg_{83.3}Cu_{7.2}Y_{9.5}$ after one cycle at 400 °C followed by rehydrogenation at 150 °C.

same as those shown in Table 2, suggesting Mg and Y did not substitute each other in this process. Therefore, the formation of polymorphic γ-MgH_2 is not related to a substitutional effect. As far as we know, this is the first observation of formation of polymorphic γ-MgH_2 through the hydrogenation of LPSO compounds, and its possible mechanism will be discussed later.

4. DISCUSSION

4.1. Structural Properties. Although the chemical composition of our sample determined by SEM−EDX analysis ($Mg_{83.8\pm0.2}Cu_{7.4\pm0.3}Y_{8.8\pm0.1}$) is close to the ideal composition of the 14*H* structure (Table 1), the XRD analysis shows that the main phase of our $Mg_{83.3}Cu_{7.2}Y_{9.5}$ is LPSO with a 18*R* structure. Here, we would like to discuss such compositional deviation from the stoichiometry of LPSO compounds.

Ternary phase diagrams for Mg−Cu−Y[33,38] and Mg−Ni−Y systems[39] were reported. Investigations of the Mg−Cu−Y system, with Mg content higher than 90 at %, have highlighted the existence of the LPSO compound with the 14*H* structure for Mg content between 90.3 and 91.7 at %.[38] This magnesium content is high compared to the ideal composition for the 14*H* structure (Table 1). In the Mg−Ni−Y system,[39] similar results were reported and Mg content is from 90.3 to 92.3 at % for 14*H*, from 84.2 to 90 at % for 18*R*, and from 78.8 to 85.7 at % for 10*H*. In all cases, LPSO contains more Mg than the stoichiometric composition. This is consistent with our present result.

Several groups attempted to explain the deviation from the ideal composition for LPSO compounds. First principle calculations suggest that the $L1_2$ type B_6A_8 clusters (Figure 1) in 14*H* $Mg_{83.3}Zn_{7.2}A_{9.5}$ and 18*R* $Mg_{80.6}Zn_{8.3}A_{11.1}$ compounds are distorted in such a way that A and Zn atoms are displaced

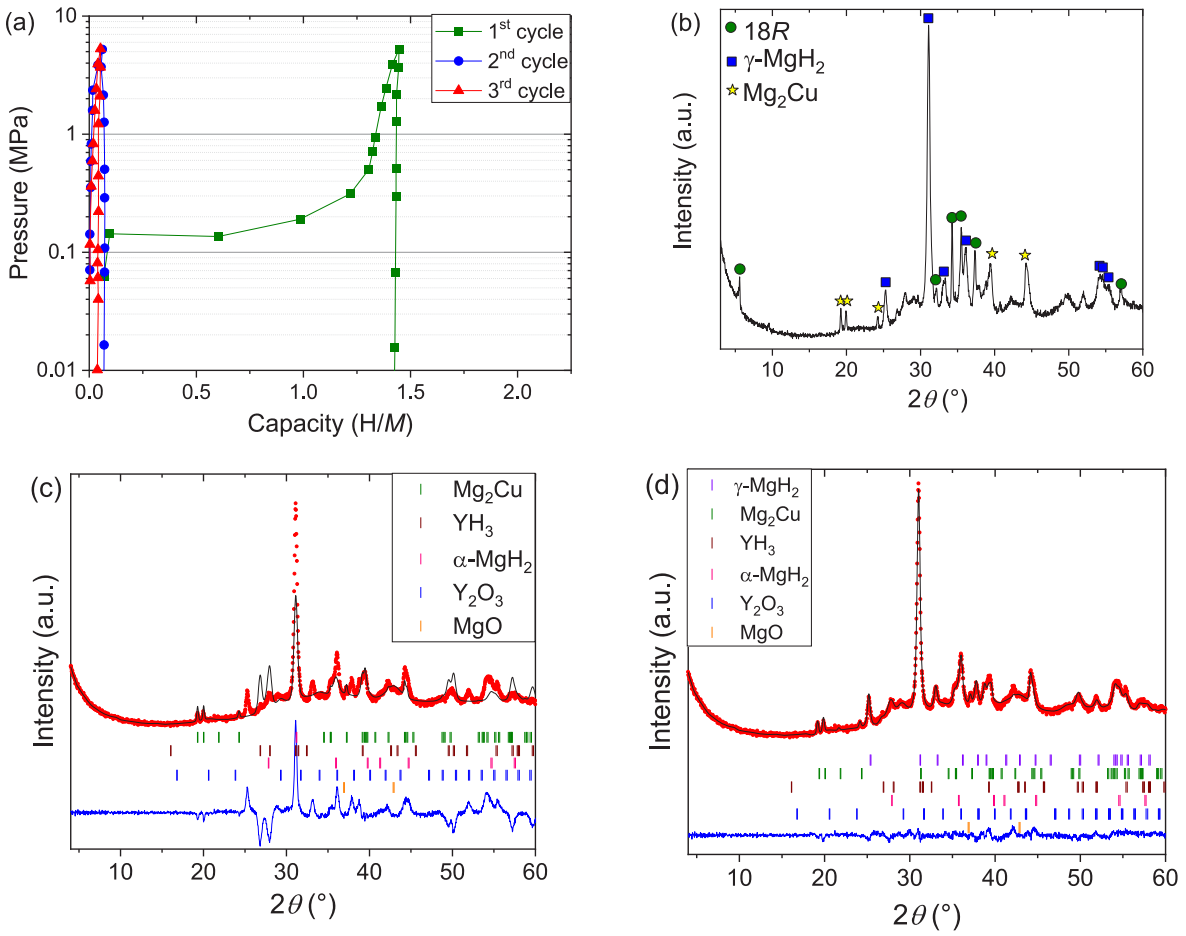

Figure 6. (a) PC isotherms for pristine $Mg_{83.3}Cu_{7.2}Y_{9.5}$ measured at 150 °C. (b) XRD patterns of $Mg_{83.3}Cu_{7.2}Y_{9.5}$ after one hydrogenation cycle at 150 °C; (c, d) after the third cycle at 150 °C, the powder was crushed in ethanol in air. The supernatant powder was used for Rietveld refinement. (c) Rietveld refinement without the addition of the γ-MgH_2 phase. The phase abundance of YH_3 is overevaluated. (d) Rietveld refinement with the addition of the γ-MgH_2 phase. The fit has been greatly improved, and the results are gathered in Table 3.

https://dx.doi.org/10.1021/acs.inorgchem.0c02080
Inorg. Chem. XXXX, XXX, XXX−XXX

Table 3. Results of Rietveld Refinement for $Mg_{83.3}Cu_{7.2}Y_{9.5}$ after Hydrogenation at 150 °C and Crushing in Ethanol (Figure 6d)[a]

	γ-MgH_2 *Pbcn*	$\Delta x/x$ (%)	Mg_2Cu *Fddd*	YH_3 $P\bar{3}c1$	α-MgH_2 $P4_2/mnm$	Y_2O_3 $Ia\bar{3}$	MgO $Fm\bar{3}m$
wt %	53.8(6)		4.3(1)	1.6(1)	11.7(3)	3.7(1)	24.9(6)
a (Å)	4.624(2)	+2.44	5.283(3)	6.36(1)	4.526(5)	10.59 (1)	4.223(6)
b (Å)	5.394(2)	−0.82	9.074(6)	*a*	*a*	*a*	*a*
c (Å)	4.964(2)	+0.48	18.34(2)	6.634(1)	3.022(7)	*a*	*a*
V (Å^3)	123.8(1)	+2.08	879.1(5)	232.3(4)	61.96(8)	1186(1)	75.29(9)
L (nm)	23(2)		*b*	*b*	*b*	*b*	*b*
ε (%)	0.61		*b*	*b*	*b*	*b*	*b*
χ^2 (%)				2.18			

[a]The column $\Delta x/x$ compares the cell parameters of γ-MgH_2 of the sample to the tabulated cell parameters of γ-MgH_2. *L* is the crystallite size (diameter); ε is the strain; χ^2 is the goodness of fit. [b]The crystallite size and strain are not given because the phase fraction is too small and/or the diffraction peaks overlap with other phases, making it difficult to obtain values with a physical meaning.

toward and outward the center of the cluster, respectively. This leads to the formation of a large interstitial site at the center of the B_6A_8 clusters.[28] These calculations also show that Mg, as interstitial atom, is the most preferred element to occupy the center of the B_6A_8 cluster.[29] If we consider that each Cu_6Y_8 cluster contains only Mg atom as interstitial atom, the Mg contents will increase to 83.7, 80.8, and 77.0 at % for 14*H*, 18*R*, and 10*H* structures, respectively. This interstitial model does not make a substantial contribution to the composition. Therefore, such a large deviation of Mg content in LPSO cannot be solely explained by occupation at the center of Cu_6Y_8 clusters.

Next, we simply consider the possibility that some of Cu_6Y_8 clusters are replaced by Mg_{14} clusters. In the 18*R* structure model, there are four Cu_6Y_8 clusters in one unit cell. If one (two) of the eight Cu_6Y_8 clusters in two unit cells is replaced, the chemical composition becomes $Mg_{83.0}Cu_{7.29}Y_{9.71}$ ($Mg_{85.42}Cu_{6.25}Y_{8.33}$). Our SEM−EDX results are close to these cases. As described above, Xu et al. showed that the composition range of Mg for 14*H* and 18*R* in the Mg−Ni−Y system are from 90.3 to 92.3 at % and from 84.2 to 90 at %, respectively.[39] In both cases, the maximum Mg content can be explained by the model where a half of Cu_6Y_8 clusters in the unit cell are replaced by Mg_{14} clusters. To further examine the phase-composition relationship of Mg−Cu−Y LPSO, we synthesized a Mg−Cu−Y compound with a higher Mg content. The SEM−EDX analysis showed a chemical composition of $Mg_{89.0\pm0.6}Cu_{5.1\pm0.2}Y_{5.9\pm0.5}$. As we expected, the crystal structure of this main phase is the 14*H* structure. This suggests that two of the Cu_6Y_8 clusters are replaced in three unit cells of the 14*H* structure and not only 18*R* but also 14*H* has more Mg in Mg−Cu−Y system. This result indicates that the LPSO phases can tolerate a large difference in their stoichiometric compositions. The replacement of B_6A_8 clusters by Mg clusters may explain it.

Now, we would like to focus on the B/A ratio. According to SEM−EDX analysis, our sample shows a B/A ratio close to 0.8 for both Mg-rich and highly Mg-rich 18*R* phases, which is slightly larger than the ideal value (0.75 = 6/8). It means that Cu content is slightly larger or Y content is slightly lower. This is in line with the results of Jiang et al.,[38] who measured a Cu/Y ratio of 0.82 ± 0.07 for the 14*H* structure in the Mg−Cu−Y system after annealing at 400 °C for 1500 h. In fact, ABF-STEM images of 18*R* and 10*H* Mg−Zn−Y showed that Mg, Y, Zn, or a vacancy occupies the interstitial site at the center of the B_6A_8 clusters.[26] The atomic radius of Cu is the smallest among our constituent elements. Therefore, the Cu/Y ratio suggests that extra Cu atoms might be inserted in the Cu_6Y_8 cluster as an interstitial atom in the Mg−Cu−Y system. If we consider two 18*R* cells and insert Cu at the center of 3 of the 8 clusters (in two 18*R* cells), the Cu/Y ratio becomes 0.80. It suggests that Cu atoms might be inserted in the B_6A_8 cluster. However, the first principle calculation for the Mg−Y−Zn system has shown that Zn is the most unstable element to occupy the center of B_6A_8 clusters, even though Zn has the smallest atomic radius among them.[26]

Another possibility is the substitution. Egusa and Abe proposed that a substitution of A and B by Mg is very likely to happen.[28] When one considers the atomic radius of Y (1.776 Å), Cu (1.278 Å), and Mg (1.599 Å), Mg is more likely to substitute Y rather than Cu (Hume−Rothery rules). Finally, we considered that one (two) of the eight Cu_6Y_8 clusters in two unit cells of the 18*R* structure is replaced by one (two) Mg_{14} cluster and that four (two) Y atoms are replaced by Mg atoms. In this case, the composition becomes $Mg_{85.76}Cu_{6.25}Y_{7.83}$ ($Mg_{83.68}Cu_{7.29}Y_{9.03}$), which is extremely close to our SEM−EDX data and explains the high Mg content as well as the high Cu/Y ratio. Our results clearly show that the high Mg content is mainly due to the substitution of Cu and Y by Mg. It would be interesting to confirm the stability of this simple LPSO structure model with the density functional theory or by confronting experimental annular bright-field scanning transmission electron micrographs to calculated ones.

4.2. Hydrogenation Reaction and Change in Crystal Structure. As shown in Figures 4 and 6, 18*R* $Mg_{83.3}Cu_{7.2}Y_{9.5}$ decomposes upon hydrogenation and the crystal structure of the resulting Mg hydride depends on the hydrogenation temperature. Here, we would like to discuss the reaction pathway and the dependence on hydrogenation temperature of the crystal structure of Mg hydride.

4.2.1. High Hydrogenation Temperature: 400 °C. The XRD pattern of the fully hydrogenated sample (Figure 4d) shows that the $Mg_{83.3}Cu_{7.2}Y_{9.5}$ LPSO compound decomposed into YH_3, α-MgH_2, and $MgCu_2$ upon hydrogenation with a maximal capacity of 1.86 H/M (4.9 wt %). This is consistent with previous studies investigating the hydrogenation of 18*R*-type Mg−Ni−Y LPSO compounds at 300−350 °C.[44,45]

The enthalpies of formation of YH_2, YH_3, and α-MgH_2 are −228, −178, and −74.5 kJ·mol^{-1} H_2, respectively.[46] Consequently, the formation of YH_2 is the most favorable and should take place prior to the formation of α-MgH_2. Such behavior was observed by Zlotea et al. for $Mg_{24}Y_5$,[46] Ishikawa et al. for $Mg_{85}Zn_6Y_9$,[47] and Li et al., who studied hydrogenation of the Mg−Ni−Y system by means of in situ synchrotron

https://dx.doi.org/10.1021/acs.inorgchem.0c02080
Inorg. Chem. XXXX, XXX, XXX−XXX

Table 4. Hydrogenation and Dehydrogenation Pathways for $Mg_{83.3}Cu_{7.2}Y_{9.5}$ at 400 °C and the Amount of Hydrogen Associated with Each Step

		hydrogen content (H/M)	
		by step	cumulative
hydrogenation pathway			
$Mg_{83.8\pm0.2}Cu_{7.4\pm0.3}Y_{8.8\pm0.1}$	→ 69Mg + 8.8YH_2 + 7.4Mg_2Cu	0.176	0.176
	→ 69α-MgH_2 + 8.8YH_3 + 7.4Mg_2Cu	1.468	1.644
	→ 80.1α-MgH_2 + 8.8YH_3 + 3.7$MgCu_2$	0.222	1.866
dehydrogenation pathway			
80.1α-MgH_2 + 8.8YH_3 + 3.7$MgCu_2$	→ 69α-MgH_2 + 8.8YH_3 + 7.4Mg_2Cu	−0.222	−0.222
	→ 69Mg + 8.8YH_2 + 7.4Mg_2Cu	−1.468	−1.690

XRD.[48] Similar results were obtained for $LaMg_{12}$, where first disproportionation of the alloy into lanthanum hydride and metallic magnesium takes place, followed by hydrogenation of Mg,[49] matching with the enthalpy of formation of each hydride. The PC isotherm of $Mg_{83.3}Cu_{7.2}Y_{9.5}$ recorded at 400 °C also follows the same steps. When one takes the average LPSO composition obtained from the SEM−EDX study, i.e., $Mg_{83.8\pm0.2}Cu_{7.4\pm0.3}Y_{8.8\pm0.1}$, its decomposition should lead to the formation of 8.8 YH_2 as the first step, which is equivalent to 0.176 H/M (Table 4). This is very close to the measured hydrogen content in the low pressure range, 0.18 H/M. Thus, Y is consumed to form YH_2 at the first step of hydrogenation. The proportions of remaining elements are 91 at % of Mg and 9 at % of Cu. According to the phase diagram of Cu−Mg,[50] in this composition range and temperature (400 °C), there is formation of Mg and Mg_2Cu, which is in good agreement with our XRD results showing YH_2, Mg, and Mg_2Cu as decomposition products (Figure 4b).

When one takes into account the enthalpy, the next reaction should be the hydrogenation of YH_2 into YH_3. However, the plateau was not observed clearly in our PC isotherms, probably because of the slow kinetics. Then, the hydrogenation of Mg into α-MgH_2 should occur at about 1.86 MPa at 400 °C (since ΔH = −74.5 kJ·mol^{-1} H_2 and ΔS = 135 J·K^{-1}·mol^{-1} H_2[16]). This is close to the plateau at 1.2 MPa and consistent with the results of Couillaud et al.[51] If YH_2 and metallic Mg are hydrogenated, the increase in hydrogen content should be 1.468 H/M. This is close to the width of this plateau in the PC isotherm (Figure 4a). The XRD analysis of $Mg_{83.3}Cu_{7.2}Y_{9.5}$ hydrogenated at 400 °C under 1.5 MPa shows that the sample mainly consists of α-MgH_2, Mg_2Cu, and YH_3 (Figure 4c and Table 2). The detection of small quantities of both Mg and YH_2 suggests that their hydrogenation into α-MgH_2 and YH_3 happens simultaneously. Therefore, this intermediate plateau is attributed to the formation of α-MgH_2 and YH_3.

At 400 °C, disproportionation of Mg_2Cu into α-MgH_2 and $MgCu_2$ occurs under 5.4 MPa of hydrogen.[30,51] This is equivalent to the absorption of 0.222 H/M (Table 4). The expected plateau pressure and capacity match well with the last plateau at 4 MPa. In fact, the XRD pattern after hydrogenation at 400 °C under 4 MPa of hydrogen pressure showed the formation of $MgCu_2$ instead of Mg_2Cu. Therefore, the last reaction corresponds to the hydrogenation of Mg_2Cu. Finally, the hydrogenation/dehydrogenation process of $Mg_{83.3}Cu_{7.2}Y_{9.5}$ at 400 °C is summarized in Table 4.

4.2.2. Formation of Polymorph of MgH_2. Surprisingly, the formation of less stable γ-MgH_2 is clearly observed after hydrogenation of $Mg_{83.3}Cu_{7.2}Y_{9.5}$ at 150 °C (Figure 6 and Table 3). In addition, the relative content of γ-MgH_2/MgH_2 is high (82%). Hydrogenation properties of LPSO phases have been investigated,[44,45,47,48] but the formation of γ-MgH_2 has not been reported. This is the first time that γ-MgH_2 is directly synthesized by a low pressure (about 0.14 MPa) and low temperature (150 °C) route with such a high content. Here, therefore, we would like to discuss the possible formation mechanism of γ-MgH_2 from the viewpoints of nanosizing, strain, and structural defects.

γ-MgH_2 is known to form through the phase transition of α-MgH_2 under very high pressure (2.5 GPa) at 250 °C as a thermally equilibrium phase.[13,17] On the other hand, the synthesis condition in the present study is about 0.14 MPa and 150 °C. According to the pressure−temperature phase diagram of MgH_2, this is far from its equilibrium condition.[17] Therefore, γ-MgH_2 formed by hydrogenation of LPSO compounds must be in a metastable state. In order to confirm it, the effect of hydrogenation temperature on the crystal structure of MgH_2 was investigated. As described in the experimental results, a high fraction of γ-MgH_2 (82%) was formed at 150 °C, while only α-MgH_2 was observed at 400 °C. When it was hydrogenated at 200 °C, clear Bragg peaks from γ-MgH_2 still appeared with those from α-MgH_2 as shown in Figure 7 but peak intensities from γ-MgH_2 decreased. The

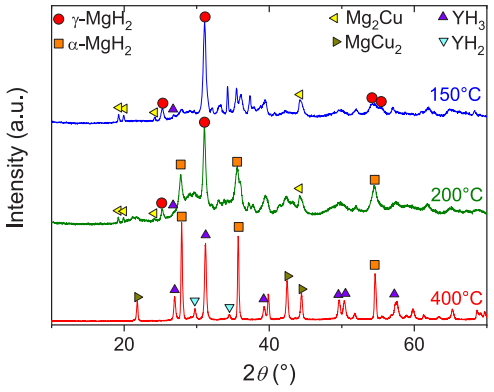

Figure 7. XRD patterns of $Mg_{83.3}Cu_{7.2}Y_{9.5}$ after hydrogenation at 150, 200, and 400 °C.

results from the Rietveld refinement are shown in Figure S2 and Table S1. The relative content of γ-MgH_2, γ-MgH_2/MgH_2, was about 50%. It is clear that the fraction of γ-MgH_2/MgH_2 depends on the temperature and that the low hydrogenation temperature promotes the formation of γ-MgH_2. These results indicate that, when hydrogenated at high temperature, LPSO forms thermodynamically stable α-MgH_2 and, when hydrogenated at low temperature, LPSO preferably forms metastable

https://dx.doi.org/10.1021/acs.inorgchem.0c02080
Inorg. Chem. XXXX, XXX, XXX−XXX

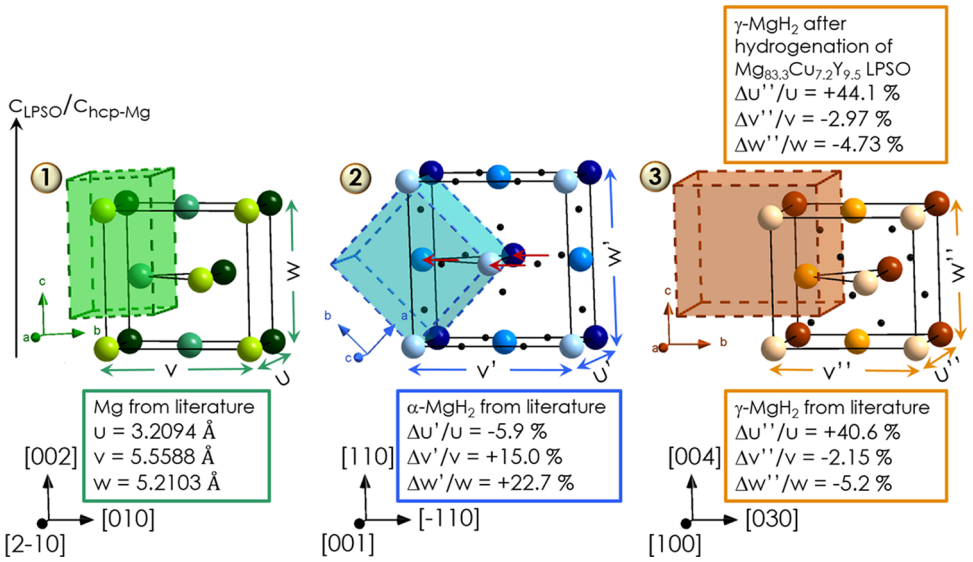

Figure 8. Crystal structures of (1) hcp Mg with $P6_3/mmc$ space group,[63] (2) tetragonal α-MgH_2 with $P4_2/mnm$ space group,[64] and (3) orthorhombic γ-MgH_2 with $Pbcn$ space group[65] and their coordination system. The large colored balls are Mg atoms; the small black balls are H atoms. The Mg atoms with light colors (light green, light blue, and light brown) belong to the front face of the cell with black edges. The dark Mg atoms are located on the back face of the cell, and the Mg atoms with intermediate color are in the intermediate plane. The cells with colored faces are the conventional cells. The vertical axis on the left represents the direction of c for the LPSO. It is parallel to the c-axis of hcp-Mg (Figure 1). The evolution of the lattice dimensions of the hydrides are compared to hcp-Mg. The three red arrows indicate the slight displacement of one atomic layer, leading to the formation of α-MgH_2.

γ-MgH_2. Therefore, an important parameter to form γ-MgH_2 via hydrogenation of LPSO compounds is the hydrogenation temperature.

Formation of metastable MgH_2 was reported by the following methods: HPT of α-MgH_2,[14] ball-milling of α-MgH_2,[1,18,19] and hydrogenation of Mg-thin films.[20−22,52−56] Edalati et al. synthesized γ-MgH_2 by HPT of α-MgH_2 at 27 °C.[14] They demonstrated that the formation of γ-MgH_2 is promoted with an increase in the applied pressure and the number of turns (deformation cycle). They explained that the formation of γ-MgH_2 was triggered by the formation of defects induced by strain. In addition, TEM analysis evidenced that HPT leads to smaller grain size (down to 70 ± 35 nm). Ball-milling also implies external mechanical deformation, and it was reported that it induced the formation of γ-MgH_2 even though the fraction is only 18 wt %.[1] Similarly to HPT, it was also concluded that the formation of γ-MgH_2 is due to the creation of strains and structural defects. Upon these mechanical deformation processes implying external stress, strain (structural defects) and/or small grain size must affect the formation of γ-MgH_2.

From here, we will discuss crystallite size and lattice strain estimated by our Rietveld refinement. When LPSO is hydrogenated at 400 °C or rehydrogenated at 150 °C after hydrogenation at 400 °C, the crystallite size and lattice strain for α-MgH_2 are 67 nm and 0.080% and 43 nm and 0.13%, respectively. Those for γ-MgH_2 hydrogenated at 150 °C are 23 nm and 0.61% (the lattice strain and crystallite size for α-MgH_2 cannot be evaluated because of the small phase fraction). Those for α-MgH_2 and γ-MgH_2 hydrogenated at 200 °C are 10 nm and 0.18% and 25 nm and 0.69%, respectively. In all cases, crystallite size for both α-MgH_2 and γ-MgH_2 are smaller than that for HPT samples.[14] Therefore, it is difficult to conclude whether there is a limitation for crystallite size to form γ-MgH_2. On the other hand, the lattice strain for γ-MgH_2 is always much higher than for α-MgH_2. Especially, α-MgH_2 resulting from hydrogenation at 400 °C contains a negligible amount of strain. Therefore, our results suggest that the key parameter to form γ-MgH_2 is lattice strain and that it affects the phase stability.

The formation of metastable orthorhombic MgH_2 (either γ-MgH_2 or $CaCl_2$-type MgH_2) was also observed upon direct hydrogenation of Mg-based thin films without external stress.[20,21,52−56] The trend that comes out is that α-MgH_2 is more likely to form when the Mg-thin film is porous or exhibits columns perpendicular to the surface, whereas the content of orthorhombic MgH_2 is higher when the film is dense. It is thought that the low porosity of the dense thin films restricts the free expansion of magnesium during its hydrogenation into MgH_2, which favors the formation of *metastable* MgH_2. In fact, Siviero et al., who hydrogenated 200 nm thick Mg-thin films at 100 °C, proposed that it was the result of compressive stress generated by clamping of the film to the substrate.[20] Nagengast et al. estimated that a stress of about 3.2 GPa was induced in their Mg-based thin films upon hydrogenation, resulting in the formation of γ-MgH_2.[22] Therefore, the spatial constraint or compressive stress is also an important factor in the formation of γ-MgH_2.

The LPSO compounds consist of infinite layers of hcp-Mg sandwiched by Mg-A-B layers and can be compared to dense Mg-thin films. It suggests the possibility of formation of metastable MgH_2 upon hydrogenation of LPSO compounds, as observed in the present work. In addition, the plane of the hcp-Mg layers, which is perpendicular to the c_{LPSO}-axis, is (002) (Figure 1), like what is usually observed for Mg-thin films. From this basis and similarly to the images shown in refs 52 and 53, we examined the relationship between hcp-Mg (1) and the magnesium hydrides, α-MgH_2 (2) and γ-MgH_2 (3) (Figure 8). The cells with black edges can easily be compared to each other, and for a better understanding, the conventional cells (with colored faces) are also represented. It turns out that, in the case of the transformation of hcp-Mg to α-MgH_2, the

https://dx.doi.org/10.1021/acs.inorgchem.0c02080
Inorg. Chem. XXXX, XXX, XXX−XXX

cell expansion is mainly parallel to $c_{hcp\text{-}Mg}$ (+22.7%) and the atoms located in the middle plane shifted following the red arrows, in good agreement with refs 52−54. As for the transformation to orthorhombic MgH_2, in the case of certain thin films, a shear deformation of the hcp-Mg cell leads to MgH_2 with a $CaCl_2$-type structure.[52,53] On the other hand, in the present study, the hcp-Mg cell expands along the $[2\bar{1}0]$ direction and slightly shrinks along the *c*-axis to form γ-MgH_2 with an α-PbO_2-type structure.

The structural relationship between hcp-Mg and γ-MgH_2 as well as the large strain observed in our γ-MgH_2 (Table 3) allow us to propose a possible mechanism for the formation of γ-MgH_2 in LPSO compounds. The hydrogenation starts in the Mg-A-B layers with the formation of YH_2. Because of the low temperature, YH_2 nucleates randomly and aggregates in each Mg-A-B layer, which results in the collapse of Cu_6Y_8 clusters. The nucleation of MgH_2 can easily occur at lattice defects or contaminating phases.[57] Therefore, the formation of MgH_2 easily takes place near the YH_2 clusters. *Local* expansion of the Mg-A-B layers, triggered by the formation of YH_2 clusters, generates compressive stress perpendicular to the Mg layers and tensile stress parallel to the Mg layers. The compressive stress prevents Mg from expanding along the *c*-axis upon hydrogenation, whereas the tensile stress favors its expansion in the (*ab*)-plane. As already shown in Figure 8 (3), a slight contraction of the cell occurs in the $c_{hcp\text{-}Mg}$ direction (−5.2%). This suggests that γ-MgH_2 is preferably formed when it is difficult for Mg to expand along the *c*-axis ([0001] direction), just like our LPSO hydrogenated at 150 °C, where the Mg layers undergo compressive stress parallel to *c*. The most significant change of the Mg cell upon formation of γ-MgH_2 occurs along the Mg [2−10] direction. This expansion is extremely large for γ-MgH_2 formed in the present study (+44%).

Note that layered-phase transformation is also reported in the similar stacking structure materials, AB_y compounds ($2 < y < 5$). The structure of AB_y compounds consists of the piling of $[AB_2]$ and $[AB_5]$ units along the *c*-axis. These compounds showed stepped hydrogenation. The $[AB_2]$ units hydrogenate to form $[AB_2H_x]$ units in the first step, and then, $[AB_5]$ units hydrogenate to form the full hydride. In the first hydrogenation step, the expansion of the $[AB_2]$ units along the *c*-axis can increase by more than 50%,[58,59] while a shrinkage of the outer part of the $[AB_5]$ units (close to the $[AB_2]$ units) was observed (down to −8% along the *c*-axis[60]). The hydrogen-induced structural change in our LPSO compounds at 150 °C is probably similar to the structural change in AB_y compounds.

The low hydrogenation temperature inhibits the release of strains, while high temperature processes can release it. Therefore, strains highlighted by X-ray diffraction analysis explain the formation of metastable γ-MgH_2 at low hydrogenation temperature and the increase in α-MgH_2 content at higher hydrogenation temperature (Figure 7). Vajeeston et al. calculated the total energy of several MgH_2 polymorphs.[61] It turns out that the difference between α- and γ-MgH_2 is very tiny (a few meV); thus, the formation of metastable γ-MgH_2 may become possible by the introduction of constraints or strains.

The presence of γ-MgH_2 is interesting because it was observed that the compounds containing γ-MgH_2 exhibit higher desorption pressure and improved kinetics compared to pure α-MgH_2.[1,15,18] This behavior is due to the low stability of γ-MgH_2 and its distorted structure, leading to enhanced hydrogen diffusion.[62] To determine the cycling properties of the metastable γ-MgH_2, differential scanning calorimetry (DSC) was carried out under hydrogen pressure (Figure S3). The XRD analysis performed after one dehydrogenation/hydrogenation cycle showed that the γ-MgH_2 phase completely disappeared and is replaced by α-MgH_2. However, the peaks for absorption and desorption are not shifted upon cycling. A detailed thermodynamic study of γ-MgH_2 is still on going.

5. CONCLUSIONS

In order to understand the effect of nanosizing of magnesium on hydrogenation properties, $Mg_{83.3}Cu_{7.2}Y_{9.5}$ was synthesized and its hydrogenation properties were investigated at different temperatures. The $Mg_{83.3}Cu_{7.2}Y_{9.5}$ LPSO compound with a 18*R* structure was successfully synthesized. At each temperature, the LPSO structure decomposed upon hydrogenation. At 400 °C, $Mg_{83.3}Cu_{7.2}Y_{9.5}$ undergoes a three-step disproportionation into α-MgH_2, YH_3, and $MgCu_2$. Interestingly, with a decrease in hydrogenation temperature, the polymorphic γ-MgH_2 phase was formed together with α-MgH_2 and the fraction of γ-MgH_2/MgH_2 reached 82% at 150 °C. We propose that the formation of γ-MgH_2 may result from a combination of several factors: first, the small difference in total energy between α-MgH_2 and γ-MgH_2; second, the structure of LPSO compounds providing regular and nanosized Mg layers; third, the inner stress rising during the hydrogenation process induced by the peculiar LPSO structure and promoted by the low hydrogenation temperature, which inhibits atomic diffusion.

■ ASSOCIATED CONTENT

Supporting Information

The Supporting Information is available free of charge at https://pubs.acs.org/doi/10.1021/acs.inorgchem.0c02080.

XRD analysis for $Mg_{83.3}Cu_{7.2}Y_{9.5}$ after hydrogenation at 150 and 200 °C; results of Rietveld refinement; DSC analysis for $Mg_{83.3}Cu_{7.2}Y_{9.5}$ after hydrogenation at 150 °C (PDF)

■ AUTHOR INFORMATION

Corresponding Author

Véronique Charbonnier − *Energy Process Research Institute, National Institute of Advanced Industrial Science and Technology (AIST), Tsukuba West, Tsukuba, Ibaraki 305-8569, Japan;* orcid.org/0000-0002-9939-2213; Email: v.charbonnier@aist.go.jp

Authors

Kohta Asano − *Energy Process Research Institute, National Institute of Advanced Industrial Science and Technology (AIST), Tsukuba West, Tsukuba, Ibaraki 305-8569, Japan;* orcid.org/0000-0003-4208-7303

Hyunjeong Kim − *Energy Process Research Institute, National Institute of Advanced Industrial Science and Technology (AIST), Tsukuba West, Tsukuba, Ibaraki 305-8569, Japan*

Kouji Sakaki − *Energy Process Research Institute, National Institute of Advanced Industrial Science and Technology (AIST), Tsukuba West, Tsukuba, Ibaraki 305-8569, Japan;* orcid.org/0000-0003-4781-1073

Complete contact information is available at: https://pubs.acs.org/10.1021/acs.inorgchem.0c02080

https://dx.doi.org/10.1021/acs.inorgchem.0c02080
Inorg. Chem. XXXX, XXX, XXX−XXX

Author Contributions

The manuscript was written through contributions of all authors. All authors have given approval to the final version of the manuscript.

Notes

The authors declare no competing financial interest.

■ ACKNOWLEDGMENTS

This work was supported by Japan Society for the Promotion of Science under a short-term program (PE18009) and International Joint Research Program for Innovative Energy Technology by the Ministry of Economy, Trade and Industry (METI).

■ REFERENCES

(1) Huot, J.; Liang, G.; Boily, S.; Van Neste, A.; Schulz, R. Structural study and hydrogen sorption kinetics of ball-milled magnesium hydride. *J. Alloys Compd.* **1999**, *293*−*295*, 495−500.
(2) Crivello, J.-C.; Denys, R. V.; Dornheim, M.; Felderhoff, M.; Grant, D. M.; Huot, J.; Jensen, T. R.; de Jongh, P.; Latroche, M.; Walker, G. S.; Webb, C. J.; Yartys, V. A. Mg-based compounds for hydrogen and energy storage. *Appl. Phys. A: Mater. Sci. Process.* **2016**, *122*, 85.
(3) Larsson, P.; Araujo, C. M.; Larsson, J. A.; Jena, P.; Ahuja, R. Role of catalysts in dehydrogenation of MgH_2 nanoclusters. *Proc. Natl. Acad. Sci. U. S. A.* **2008**, *105*, 8227−8231.
(4) Zaluska, A.; Zaluski, L.; Strom-Olsen, J. O. Nanocrystalline magnesium for hydrogen storage. *J. Alloys Compd.* **1999**, *288*, 217−225.
(5) Zlotea, C.; Latroche, M. Role of nanoconfinement on hydrogen sorption properties of metal nanoparticles hybrids. *Colloids Surf., A* **2013**, *439*, 117−130.
(6) Oelerich, W.; Klassen, T.; Bormann, R. Metal oxides as catalysts for improved hydrogen sorption in nanocrystalline Mg-based materials. *J. Alloys Compd.* **2001**, *315*, 237−242.
(7) Cheng, Y.; Zhang, W.; Liu, J.; Cheng, K.; Zhao, Z. Effect of the nanometric $LiFeO_4$ on the hydrogen storage properties of MgH_2. *Int. J. Hydrogen Energy* **2017**, *42*, 356−365.
(8) Liang, G.; Huot, J.; Boily, S.; Van Neste, A.; Schulz, R. Catalytic effect of transition metals on hydrogen sorption in nanocrystalline ball milled MgH_2-Tm (Tm = Ti, V, Mn, Fe and Ni) systems. *J. Alloys Compd.* **1999**, *292*, 247−252.
(9) Aguey-Zinsou, K.-F.; Ares Fernandez, J. R.; Klassen, T.; Bormann, R. Using MgO to improve the (de)hydriding properties of magnesium. *Mater. Res. Bull.* **2006**, *41*, 1118−1126.
(10) Manivasagam, T. G.; Kiraz, K.; Notten, P. H. L. Electrochemical and Optical Properties of Magnesium-Alloy Hydrides Reviewed. *Crystals* **2012**, *2*, 1410−1433.
(11) Bortz, M.; Bertheville, B.; Bottger, G.; Yvon, K. Structure of the high pressure phase 1-MgH_2 by neutron powder diffraction. *J. Alloys Compd.* **1999**, *287*, L4−L6.
(12) Vajeeston, P.; Ravindran, P.; Hauback, B. C.; Fjellvag, H.; Kjekshus, A.; Furuseth, S.; Hanfland, M. Structural stability and pressure-induced phase transitions in MgH_2. *Phys. Rev. B: Condens. Matter Mater. Phys.* **2006**, *73*, 224102.
(13) Bastide, J.-P.; Bonnetot, B.; Letoffe, J.-M.; Claudy, P. Polymorphisme de l'hydrure de magnésium sous haute pression. *Mater. Res. Bull.* **1980**, *15*, 1215−1224.
(14) Edalati, K.; Kitabayashi, K.; Ikeda, Y.; Matsuda, J.; Lia, H.-W.; Tanaka, I.; Akiba, E.; Horita, Z. Bulk nanocrystalline gamma magnesium hydride with low dehydrogenation temperature stabilized by plastic straining via high-pressure torsion. *Scr. Mater.* **2018**, *157*, 54−57.
(15) Zhou, S.; Zhang, Q.; Chen, H.; Zang, X.; Zhou, X.; Wang, R.; Jiang, X.; Yang, B.; Jiang, R. Crystalline structure, energy calculation and dehydriding thermodynamics of magnesium hydride from reactive milling. *Int. J. Hydrogen Energy* **2015**, *40*, 11484−11490.
(16) Stampfer, J. F.; Holley, C. E.; Suttle, J. F. The Magnesium-Hydrogen System. *J. Am. Chem. Soc.* **1960**, *82*, 3504−3508.
(17) Moser, D.; Baldissin, G.; Bull, D. J.; Riley, D. J.; Morrison, I.; Ross, D. K.; Oates, W. A.; Noreus, D. The pressure-temperature phase diagram of MgH_2 and isotopic substitution. *J. Phys.: Condens. Matter* **2011**, *23*, 305403.
(18) Varin, R. A.; Czujko, T.; Wronski, Z. Particle size, grain size and -MgH_2 effects on the desorption properties of nanocrystalline commercial magnesium hydride processed by controlled mechanical milling. *Nanotechnology* **2006**, *17*, 3856−3865.
(19) Rizo-Acosta, P.; Cuevas, F.; Latroche, M. Hydrides of early transition metals as catalysts and grain growth inhibitors for enhanced reversible hydrogen storage in nanostructured magnesium. *J. Mater. Chem. A* **2019**, *7*, 23064−23075.
(20) Siviero, G.; Bello, V.; Mattei, G.; Mazzoldia, P.; Battaglin, G.; Bazzanella, N.; Checchetto, R.; Miotello, A. Structural evolution of Pd-capped Mg thin films under H_2 absorption and desorption cycles. *Int. J. Hydrogen Energy* **2009**, *34*, 4817−4826.
(21) Gautam, Y. K.; Chawla, A. K.; Walia, R.; Agrawal, R. D.; Chandra, R. Hydrogenation of Pd-capped Mg thin films prepared by DC magnetron sputtering. *Appl. Surf. Sci.* **2011**, *257*, 6291−6295.
(22) Nagengast, D. G.; van Gogh, A. T. M.; Kooij, E. S.; Dam, B.; Griessen, R. Contrast enhancement of rare-earth switchable mirrors through microscopic shutter effect. *Appl. Phys. Lett.* **1999**, *75*, 2050.
(23) Lu, F.; Ma, A.; Jiang, J. Review on long-period stacking-ordered structures in Mg-Zn-RE alloys. *Rare Met.* **2012**, *31*, 303−310.
(24) Abe, E.; Ono, A.; Itoi, T.; Yamasaki, M.; Kawamura, Y. Polytypes of long-period stacking structures synchronized with chemical order in a dilute Mg-Zn-Y alloy. *Philos. Mag. Lett.* **2011**, *91*, 690−696.
(25) Yokobayashi, H.; Kishida, K.; Inui, H.; Yamasaki, M.; Kawamura, Y. Enrichment of Gd and Al atoms in the quadruple close packed planes and their in-plane long-range ordering in the long period stacking-ordered phase in the Mg-Al-Gd system. *Acta Mater.* **2011**, *59*, 7287−7299.
(26) Kishida, K.; Nagai, K.; Matsumoto, A.; Yasuhara, A.; Inui, H. Crystal structures of highly-ordered long-period stacking-ordered phases with 18*R*, 14*H* and 10*H*-type stacking sequences in the Mg-Zn-Y system. *Acta Mater.* **2015**, *99*, 228−239.
(27) Yamasaki, M.; Matsushita, M.; Hagihara, K.; Izuno, H.; Abe, E.; Kawamura, Y. Highly ordered 10*H*-type long-period stacking order phase in a Mg-Zn-Y ternary alloy. *Scr. Mater.* **2014**, *78*−*79*, 13−16.
(28) Egusa, D.; Abe, E. The structure of long period stacking/order Mg-Zn-RE phases with extended non-stoichiometry ranges. *Acta Mater.* **2012**, *60*, 166−178.
(29) Saal, J. E.; Wolverton, C. Thermodynamic stability of Mg-based ternary long-period stacking ordered structures. *Acta Mater.* **2014**, *68*, 325−338.
(30) Karty, A.; Grunzweig-Genossar, J.; Rudman, P. S. Hydriding and dehydriding kinetics of Mg in a Mg/Mg_2Cu eutectic alloy: Pressure sweep method. *J. Appl. Phys.* **1979**, *50*, 7200−7209.
(31) Si, T. Z.; Liu, Y. F.; Zhang, Q. A. Hydrogen storage properties of the supersaturated $Mg_{12}YNi$ solid solution. *J. Alloys Compd.* **2010**, *507*, 489−493.
(32) Kalinichenka, S.; Rontzsch, L.; Riedl, T.; Gemming, T.; Weißgarber, T.; Kieback, B. Microstructure and hydrogen storage properties of melt-spun Mg-Cu-Ni-Y alloys. *Int. J. Hydrogen Energy* **2011**, *36*, 1592−1600.
(33) Chen, R.; Ding, X.; Chen, X.; Li, X.; Su, Y.; Guo, J.; Ding, H.; Fu, H. In-situ hydrogen-induced evolution and de/hydrogenation behaviors of the $Mg_{93}Cu_{7-x}Y_x$ alloys with equalized LPSO and eutectic structure. *Int. J. Hydrogen Energy* **2019**, *44*, 21999−22010.
(34) Rodriguez-Carvajal, J. Recent advances in magnetic structure determination by neutron powder diffraction. *Phys. B* **1993**, *192*, 55−69.
(35) Rietveld, H. M. A Profile Refinement Method for Nuclear and Magnetic Structures. *J. Appl. Crystallogr.* **1969**, *2*, 65−71.
(36) Okuda, H.; Horiuchi, T.; Tsukamoto, T.; Ochiai, S.; Yamasaki, M.; Kawamura, Y. Evolution of long-period stacking ordered

https://dx.doi.org/10.1021/acs.inorgchem.0c02080
Inorg. Chem. XXXX, XXX, XXX−XXX

structures on annealing as-cast $Mg_{85}Y_9Zn_6$ alloy ingot observed by synchrotron radiation small-angle scattering. *Scr. Mater.* **2013**, *68*, 575−578.
(37) Le Bail, A. Whole powder pattern decomposition methods and applications: A retrospection. *Powder Diffr.* **2005**, *20*, 316−326.
(38) Jiang, M.; Su, X.; Li, H.; Ren, Y.; Qin, G. The phase equilibria and thermal stability of the long-period stacking ordered phase in the Mg-Cu-Y system. *J. Alloys Compd.* **2014**, *593*, 141−147.
(39) Xu, K.; Liu, S.; Huang, D.; Du, Y. Experimental investigation of the isothermal section of the Mg-Ni-Y system with LPSO phases at 400°C. *J. Mater. Sci.* **2018**, *53*, 9243−9257.
(40) Latroche, M.; Kalisvaart, P.; Notten, P. H. L. Crystal structure of $Mg_{0.65}Sc_{0.35}D_x$ deuterides studied by X-ray. *J. Solid State Chem.* **2006**, *179*, 3024−3032.
(41) Asano, K.; Kim, H.; Sakaki, K.; Jimura, K.; Hayashi, S.; Nakamura, Y.; Ikeda, K.; Otomo, T.; Machida, A.; Watanuki, T. Structural Variation of Self-Organized Mg Hydride Nanoclusters in Immiscible Ti Matrix by Hydrogenation. *Inorg. Chem.* **2018**, *57*, 11831−11383.
(42) Kataoka, R.; Kimura, T.; Takeichi, N.; Kamegawa, A. Stabilization of Face-Centered Cubic High-Pressure Phase of REH_3 (RE = Y, Gd, Dy) at Ambient Pressure by Alkali or Alkaline-Earth Substitution. *Inorg. Chem.* **2018**, *57*, 4686−4692.
(43) Yartys, V. A.; Gutfleisch, O.; Panasyuk, V. V.; Harris, I. R. Desorption characteristics of rare earth (R) hydrides (R = Y, Ce, Pr, Nd, Sm, Gd and Tb) in relation to the HDDR behaviour of R-Fe-based compounds. *J. Alloys Compd.* **1997**, *253*−*254*, 128−133.
(44) Zhang, Q. A.; Liu, D. D.; Wang, Q. Q.; Fang, F.; Sun, D. L.; Ouyang, L. Z.; Zhu, M. Superior hydrogen storage kinetics of $Mg_{12}YNi$ alloy with a long-period stacking ordered phase. *Scr. Mater.* **2011**, *65*, 233−236.
(45) Liu, J. W.; Zou, C. C.; Wang, H.; Ouyang, L. Z.; Zhu, M. Facilitating de/hydrogenation by long-period stacking ordered structure in Mg based alloys. *Int. J. Hydrogen Energy* **2013**, *38*, 10438−10445.
(46) Zlotea, C.; Lu, J.; Andersson, Y. Formation of one-dimensional MgH_2 nano-structures. *J. Alloys Compd.* **2006**, *426*, 357−362.
(47) Ishikawa, K.; Kawasaki, T.; Yamada, Y. Hydrogenation behavior of $Mg_{85}Zn_6Y_9$ crystalline alloy with long period stacking ordered structure. *Int. J. Hydrogen Energy* **2015**, *40*, 13014−13021.
(48) Li, Y.; Gu, Q.; Li, Q.; Zhang, T. In-situ synchrotron X-ray diffraction investigation on hydrogen-induced decomposition of long period stacking ordered structure in Mg-Ni-Y system. *Scr. Mater.* **2017**, *127*, 102−107.
(49) Poletaev, A. A.; Denys, R. V.; Solberg, J. K.; Tarasov, B. P.; Yartys, V. A. Microstructural optimization of $LaMg_{12}$ alloy for hydrogen storage. *J. Alloys Compd.* **2011**, *509S*, S633−S639.
(50) Mezbahul-Islam, M.; Kevorkov, D.; Medraj, M. The equilibrium phase diagram of the magnesium-copper-yttrium system. *J. Chem. Thermodyn.* **2008**, *40*, 1064−1076.
(51) Couillaud, S.; Gaudin, E.; Andrieux, J.; Gorsse, S.; Gayot, M.; Bobet, J. L. Study of the hydrogenation mechanism of $LaCuMg_8$ ternary phase: The decomposition induces kinetics improvement. *Int. J. Hydrogen Energy* **2012**, *37*, 11824−11834.
(52) Ham, B.; Junkaew, A.; Arroyave, R.; Chen, J.; Wang, H.; Wang, P.; Majewski, J.; Park, J.; Zhou, H.-C.; Arvapally, R. K.; Kaipa, U.; Omary, M. A.; Zhang, X. Y.; Ren, Y.; Zhang, X. Hydrogen sorption in orthorhombic Mg hydride at ultra-low temperature. *Int. J. Hydrogen Energy* **2013**, *38*, 8328−8341.
(53) Ham, B.; Junkaew, A.; Arroyave, R.; Park, J.; Zhou, H.-C.; Foley, D.; Rios, S.; Wang, H.; Zhang, X. Size and stress dependent hydrogen desorption in metastable Mg hydride films. *Int. J. Hydrogen Energy* **2014**, *39*, 2597−2607.
(54) Tan, Z.; Chiu, C.; Heilweil, E. J.; Bendersky, L. A. Thermodynamics, kinetics and microstructural evolution during hydrogenation of iron-doped magnesium thin films. *Int. J. Hydrogen Energy* **2011**, *36*, 9702−9713.
(55) Higuchi, K.; Yamamoto, K.; Kajioka, H.; Toiyama, K.; Honda, M.; Orimo, S.; Fujii, H. Remarkable hydrogen storage properties in three-layered Pd/Mg/Pd thin films. *J. Alloys Compd.* **2002**, *330*−*332*, 526−530.
(56) Le-Quoc, H.; Lacoste, A.; Miraglia, S.; Bechu, S.; Bes, A.; Laversenne, L. MgH_2 thin films deposited by one-step reactive plasma sputtering. *Int. J. Hydrogen Energy* **2014**, *39*, 17718−17725.
(57) Mooij, L.; Dam, B. Hysteresis and the role of nucleation and growth in the hydrogenation of Mg nanolayers. *Phys. Chem. Chem. Phys.* **2013**, *15*, 2782−2792.
(58) Yartys, V. A.; Riabov, A. B.; Denys, R. V.; Sato, M.; Delaplane, R. G. Novel intermetallic hydrides. *J. Alloys Compd.* **2006**, *408*−*412*, 273−279.
(59) Iwase, K.; Sakaki, K.; Nakamura, Y.; Akiba, E. Phase Transformation and Crystal Structure of $La_2Ni_7H_x$ Studied by in situ X-ray Diffraction. *Inorg. Chem.* **2010**, *49*, 8763−8768.
(60) Charbonnier, V.; Zhang, J.; Monnier, J.; Goubault, L.; Bernard, P.; Magen, C.; Serin, V.; Latroche, M. Structural and hydrogen storage properties of Y_2Ni_7 deuterides studied by neutron powder diffraction. *J. Phys. Chem. C* **2015**, *119*, 12218−12225.
(61) Vajeeston, P.; Ravindran, P.; Kjekshus, A.; Fjellvag, H. Pressure-Induced Structural Transitions in MgH_2. *Phys. Rev. Lett.* **2002**, *89*, 175506.
(62) Shen, C.; Aguey-Zinsou, K.-F. Can 6-MgH_2 improve the hydrogen storage properties of magnesium? *J. Mater. Chem. A* **2017**, *5*, 8644−8652.
(63) Busk, R. S. Effect of Temperature on the Lattice Parameters of Magnesium Alloys. *JOM* **1952**, *4*, 207−209.
(64) Haschke, J. M.; Clark, M. R. Phase equilibria and crystal growth of alkaline earth and lanthanide dihydrides. *High Temp. Sci.* **1975**, *7*, 152−158.
(65) Moriwaki, T.; Akahama, Y.; Kawamura, H.; Nakano, S.; Takemura, K. Structural phase transition of rutile-type MgH_2 at high pressures. *J. Phys. Soc. Jpn.* **2006**, *75*, 074603-1−074603-6.

https://dx.doi.org/10.1021/acs.inorgchem.0c02080
Inorg. Chem. XXXX, XXX, XXX−XXX